THE JOURNAL OF PHYSICAL CHEMISTRY B

ARTICLE

pubs.acs.org/JPCB

Molecular Simulation of Gas Adsorption, Diffusion, and Permeation in Hydrated Nafion Membranes

Shuai Ban, Cheng Huang,* Xiao-Zi Yuan, and Haijiang Wang

Institute for Fuel Cell Innovation, National Research Council of Canada, 4250 Wesbrook Mall, Vancouver, British Columbia V6T 1W5, Canada

ABSTRACT: Molecular simulations were performed to characterize hydrated Nafion membranes in terms of gas adsorption, diffusion, and permeation. The experimental results validate the molecular model of Nafion with respect to material density, morphology, free volume, and water diffusivity. Nafion's adsorption property is examined in terms of the solubility and adsorption isotherms for gases, including H_2, O_2, and N_2. The adsorption capacity of hydrated Nafion is shown to be strong for O_2 and N_2 but not for H_2. Due to the dilution effect, N_2 is able to suppress the loading of O_2 and protect the fuel cell from fuel crossover. The dynamic behaviors of H_2 and O_2 are represented by self-diffusion coefficients, with the results showing that H_2 diffusion in Nafion membranes is nearly 1 order of magnitude faster than O_2 diffusion. The effects of water content and the concentration of adsorbed gases were verified, and a close correlation of Nafion free volume to gas transport properties was revealed. On the basis of the solution-diffusion mechanism, the permeabilities of H_2 and O_2 in hydrated Nafion membranes are calculated and compared with corresponding experiments, and the permeability of H_2 is found to be approximately twice that of O_2.

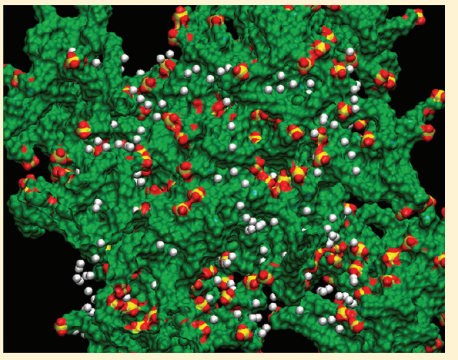

1. INTRODUCTION

During recent decades, fuel cells have been developed as an alternative energy source for transportation and stationary power applications, yielding high energy efficiency and low pollution.[1] In the field of electric vehicle applications, polymer electrolyte membrane (PEM) fuel cells are most promising due to their high power density, simple construction, and long lifetimes.[2] To date, the perfluorosulfonated polymer Nafion membranes developed by DuPont de Nemours are the most popular type of membrane in PEM fuel cell applications.[3] Besides their proton conductivity, another important property of Nafion membranes is the gas permeability, as high permeation rates of H_2/O_2 through membranes can significantly compromise a fuel cell's electrochemical performance and longevity.[4] Gas permeability is impacted by many factors. Chiou and Paul performed permeation measurements with a wide range of gases on dry Nafion 117 membranes. The permeability was $N_2 < O_2 < H_2$, and the permeation selectivity of O_2 in O_2/N_2 mixtures was slightly higher than one.[5] Broka and Ekdunge showed that O_2 permeability through a Nafion 117 membrane increases with temperature and relative humidity or water content and that H_2 permeability is about twice that of O_2.[6] Moreover, Sakai et al. pointed out that the gas permeability of Nafion greatly depends not only on water content but also on cation form and ion-exchange capacity.[7] The observed correlation of H_2/O_2 permeabilities is in line with the findings from Broka and Ekdunge[6]

Molecular simulations have also been extensively applied to study the properties of Nafion membranes.[8−13] In these studies, molecular models of Nafion have been successfully developed and experimentally validated in terms of membrane density, Nafion morphology, and water diffusivity. For gas separation, however, few papers discuss the permeation issues of Nafion because of the difficulties in simulating the complex Nafion system. Although H_2/O_2 permeabilities through Nafion membrane have been experimentally investigated to a large extent, there still exists a gap between experimental finding and theoretical understanding. Modeling approaches for describing gas permeation through membrane systems have not been well developed and validated in comparison with experimental results, especially when considering complex microstructures of polymer systems. In the present work, we attempt to tackle this issue by systematic simulation and validation of gas permeation in hydrated Nafion membranes. The water content and concentration of adsorbed gases were addressed as two important factors. A deep insight into the gas transport will be gained for Nafion at a molecular level.

2. SIMULATION METHODS

2.1. Molecular Models. The chemical structure of a Nafion polymer is shown in Figure 1. In this study, we consider a Nafion polymer that consists of 20 monomers, namely, 20 side chains, and 300 CF_x groups in the poly(tetrafluoroethylene) (PTFE) backbone. In total, 16 Nafion chains are used for all of the simulations. By assuming complete deprotonation of sulfonic acid groups in Nafion side chains, 20 hydronium ions (H_3O^+) are

Received: May 4, 2011
Revised: August 26, 2011
Published: August 29, 2011

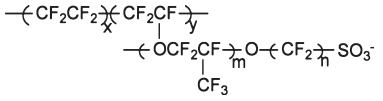

Figure 1. Chemical structure of Nafion polymer. The equivalent weight of the Nafion model is about 1100 g of dry Nafion/(mol of sulfonic acid groups), with $x = 6.5$, $y = m = 1$, and $n = 2$.

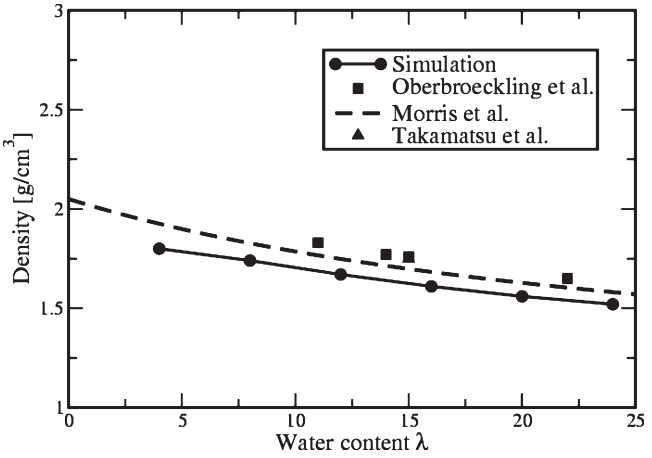

Figure 2. Densities of hydrated Nafion membranes as a function of water content. Simulations were performed at 353.15 K and 1 bar, and results are compared with experimental data taken from Morris and Sun,[31] Oberbroeckling et al.,[32] and Takamatsu and Eisenberg.[33] Note that one data point from Takamatsu and Eisenberg is overlapped with that from Oberbroeckling et al. at $\lambda = 15$.

added for each Nafion chain to maintain charge neutrality. The concentration of water in the simulation box is quantified by the factor λ, i.e. the number of water molecules per sulfonic acid group of the Nafion side chain. The force fields of Nafion and hydronium ions are taken from Venkatnathan et al.[13] A hydrated Nafion system is then achieved by inserting into the simulation box a certain number of water molecules given the factor λ. In this study, we consider water contents of $\lambda = 4$, 8, 12, 16, 20, and 24, which correspond to 6.3, 11.9, 16.8, 21.1, 25.2, and 28.8 wt %, respectively. The water molecule is simulated using the SPC/E model.[14] Similar to the setup of water molecules, a certain number of gases, including H_2, O_2, and N_2, are inserted randomly into the simulation box for the computation of gas permeation. Accordingly, the concentration of gases in Nafion membrane is denoted here as λ_{gas}, i.e., the number of gas molecules per sulfonic acid group of the Nafion side chain. The Lennard-Jones (LJ) interaction parameters of H_2 are taken from Krishna and van Baten,[15] and the parameters of single-site O_2 and N_2 models are referred to by Krishnamurthy et al.[16] The Lorentz−Bertelot mixing rule is adopted for interactions between different types of atoms. Long-range electrostatic interactions are calculated using the particle-mesh Ewald method with a fourth-order interpolation.

2.2. Simulation Procedures. To imitate Nafion's equilibrium structures, molecular dynamics (MD) simulations were employed using GROMACS software.[17−20] The initial configurations were generated by arbitrarily placing molecules in a simulation box. Periodic boundary condition is applied in all directions. To eliminate initial bias in the system, an MD simulation under an *NPT* ensemble was carried out at 800 K and 50−100 MPa using the LJ potential parameters, ε, of all

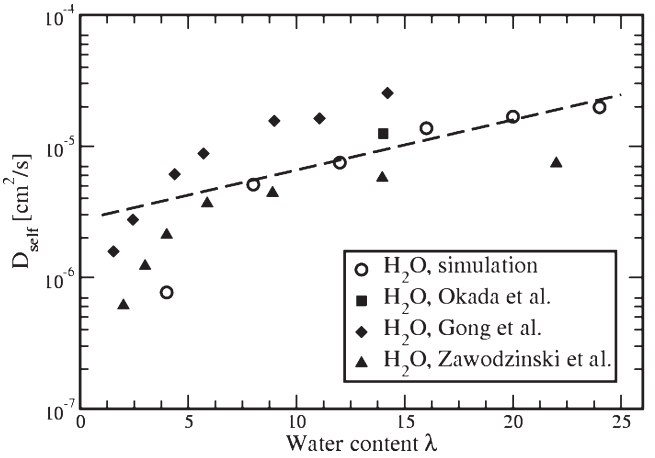

Figure 3. Self-diffusion coefficients of water in hydrated Nafion membranes. Simulations were performed at 353.15 K and 1 bar. Simulation results are compared with experimental data taken from Gong et al. at 357 K,[35] Okada et al. at 353.15 K,[36] and Zawodzinski et al. at 303.15 K.[37] The dashed lines are linear fitting of simulated D_{self} in the range $\lambda = 8-24$.

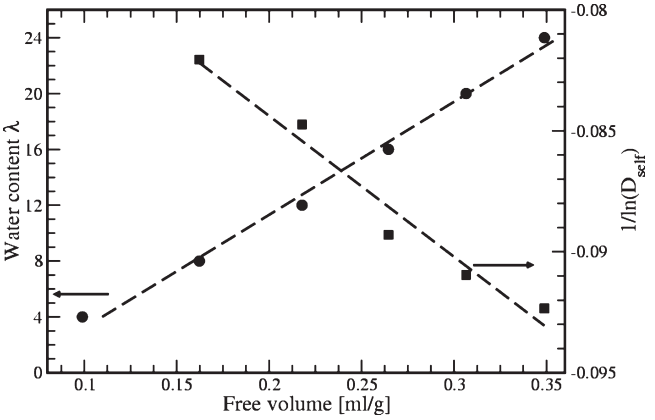

Figure 4. Free volumes of hydrated Nafion membranes in correlation with water content and self-diffusivity. Simulations were performed at 353.15 K and 1 bar. The dashed line is a linear fitting of simulation results.

Nafion atoms, reduced by 2 orders of magnitude. After that, another simulation was performed to gradually return the LJ parameters to their original values and the conditions to $T = 353.15$ K and $P = 1$ bar. In this way, a random configuration was obtained. For the annealing procedure, MD simulations were performed by varying the temperature six times between 353.15 and 800 K for 300 ps, followed by an equilibration *NPT* MD simulation at $T = 353.15$ K and $P = 1$ bar for 5 ns. The process was repeated three times to reach the equilibrium state of the Nafion system. The final structure was then used for the production *NPT* MD run at $T = 353.15$ K and $P = 1$ bar for 20 ns. The trajectory of gas molecules was collected every 20 ps for the calculation of gas diffusivities. The temperature was held by the Nosé−Hoover thermostat,[21,22] and the pressure was controlled isotropically by the Berendsen method.[19] It has been demonstrated that the characteristic microstructure of Nafion can be reasonably reproduced by using this type of MD simulations.[9−11,23] The concept of membrane free volume is adopted to characterize the porous

dx.doi.org/10.1021/jp204141b |J. Phys. Chem. B 2011, 115, 11352–11358

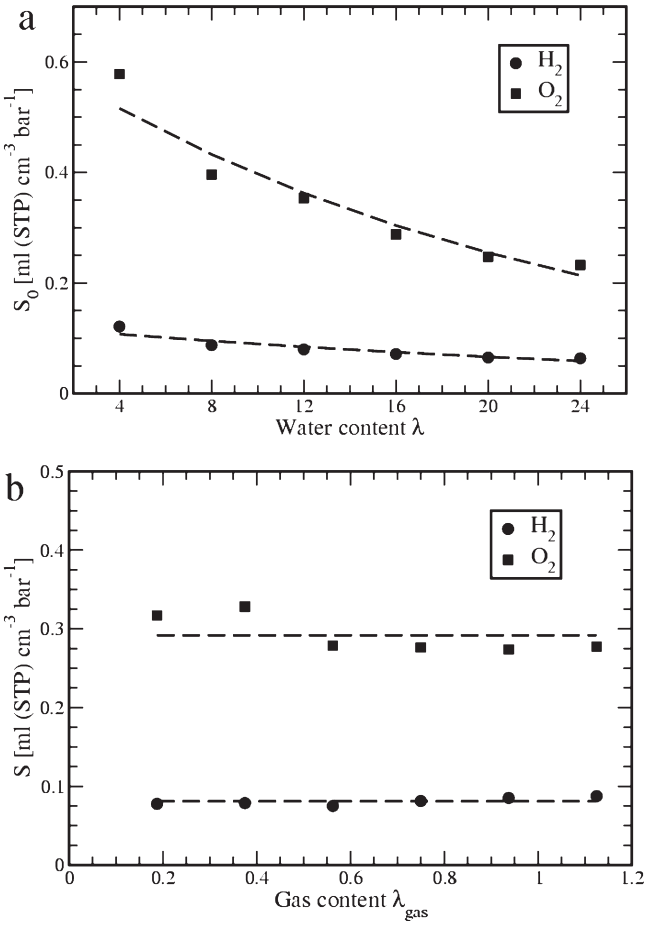

Figure 5. (a) Gas solubility coefficients at 353.15 K and zero-pressure limit for hydrated Nafion membranes. The dashed lines are exponential fitting of simulation results. (b) Gas solubility coefficients with various gas contents at 353.15 K in hydrated Nafion membranes with a constant water content of $\lambda = 12$. The dashed lines are linear fitting of simulation results.

structure of hydrated Nafion. Free volume, V_f, is an important parameter to quantify the fraction of the volume not occupied by the polymer. The free volume was computed by the simulation algorithm developed by Ban and Vlugt[24] and averaged from five configurations that were extracted from *NVT* MD simulations of equilibrated Nafion membranes running for 5 ns.

2.3. Computational Theories. On the basis of the resulting structure of equilibrated Nafion obtained from previous *NVT* MD simulation, the solubility coefficients of gases in Nafion membranes were calculated by using Widom's test-particle insertion method.[25−27] In this method, a test particle is randomly inserted into an equilibrated Nafion configuration, and the energy ΔU is calculated from the interaction between the test particle and all of the other atoms in the system. The excess chemical potential μ_{ex} follows as

$$\mu_{ex} = -k_B T \ln\left\langle \exp\left(-\frac{\Delta U}{k_B T}\right)\right\rangle \quad (1)$$

where k_B is Boltzmann's constant, ΔU is the energy change induced by inserting the test particle, T is the temperature, and $\langle ... \rangle$ is the ensemble average over all of the configurations. The chemical potential, μ_0, of test particles—i.e., O_2, H_2, and N_2—in the ideal gas phase is ignored. For each simulation, we performed

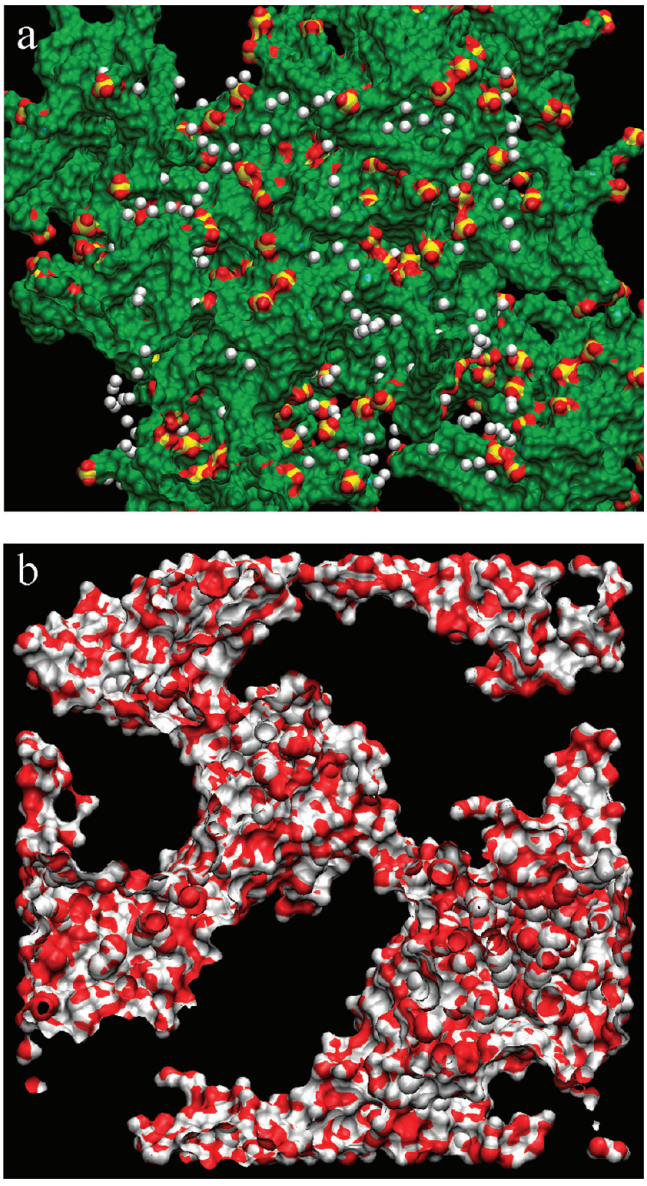

Figure 6. (a) Snapshot of O_2 in hydrated Nafion membrane with a constant water content of $\lambda = 12$ at 353.15 K. O_2 is represented by the white bead. For Nafion, the PTFE backbone is in green, the sulfonic acid group is visualized as S in yellow, and O is in red. Water molecules are removed from the membrane. Periodic boundary condition is not applied. (b) Snapshot of water domains in hydrated Nafion membrane with a content of $\lambda = 12$ at 353.15 K. O is in red, and H is white.

the particle insertion in totally 100 configurations that were collected from *NVT* MD simulations of the equilibrated Nafion system running for 5 ns. To obtain reliable statistics, 10^7 insertions were attempted for each configuration. The solubility coefficient was then obtained from

$$S = \frac{1}{k_B T} \exp\left(-\frac{\mu_{ex}}{k_B T}\right) \quad (2)$$

With consideration at temperature T and pressure P, a real gas is in equilibrium with a polymer phase at a loading q. The solubility coefficient is thus defined as $S = q/P$. Since different experimental methods are used to determine gas solubilities, they have been

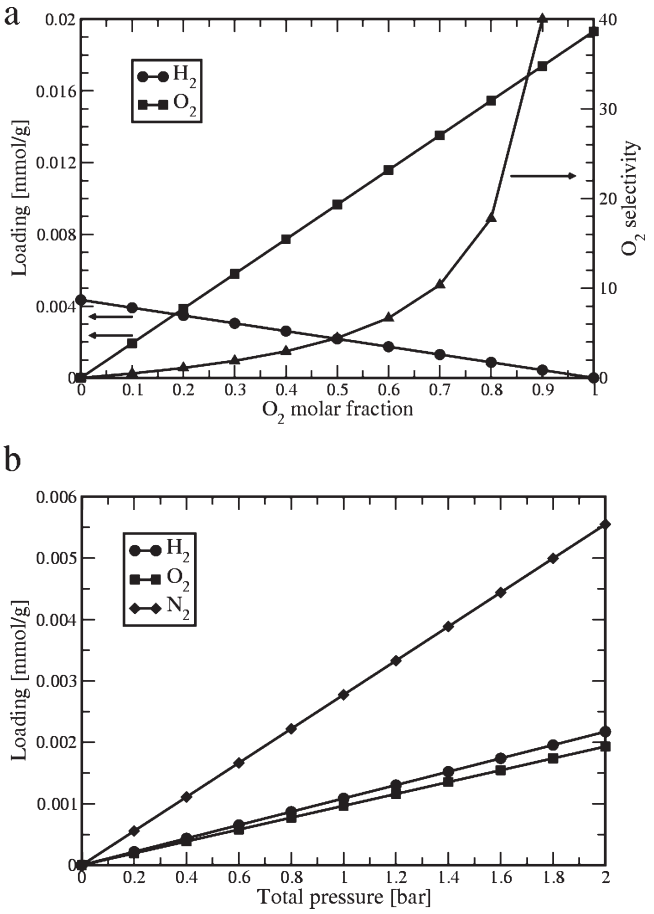

Figure 7. (a) Adsorption isotherms and selectivity of H_2/O_2 binary mixture at 353.15 K and a total pressure of 2 bar in a hydrated Nafion membrane with a constant water content of $\lambda = 12$. The adsorption isotherm of gas mixture is calculated from adsorption isotherms of single components, using the ideal adsorbed solution theory. (b) Adsorption isotherm of the $H_2/O_2/N_2$ ternary mixture at 353.15 K in the hydrated Nafion membrane with a constant water content of $\lambda = 12$. The molar fraction was fixed at H_2:O_2:N_2 = 5:1:4 in the gas phase, analogous to fuel cell gas feeding conditions. The adsorption isotherm of the gas mixture is calculated from adsorption isotherms of single components, using ideal adsorbed solution theory.

expressed in various units. One of the most often used units is the volume of gas (in the unit of milliliters) under standard conditions dissolved in 1 cm^3 polymer under a given P, which is read as

$$S = \frac{V_{gas}(\mathrm{STP})}{V_{polymer}P} \tag{3}$$

where V_{gas} is the adsorbed volume of gas at standard condition, i.e., $T_0 = 273$ K and $P_0 = 1$ atm, and $V_{polymer}$ is the volume of the polymer at temperature T and pressure P.[26] It is known that gas loadings of Nafion membranes are extremely low under fuel cell operating conditions (e.g., 353.15 K and 1 bar).[28] It is reasonable to assume that Henry's law is applicable to these dilute systems, meaning the loading of the guest molecule is proportional to its pressure in the gas phase. The adsorption isotherm is read as

$$q = k_H P \tag{4}$$

where q is the loading of gas molecules in the membrane, P is the pressure, and k_H is the Henry coefficient identical to the solubility coefficient at low loadings. The adsorption isotherm of gas mixtures is estimated by ideal adsorbed solution theory using isotherms of single components.[29]

According to Graham, the permeation of gases through polymer membranes obeys a solution diffusion mechanism. It was assumed by this theory that driven by the pressure difference across the membrane, gas molecules dissolve in the upstream side of a membrane, diffuse through the membrane, and desorb from the downstream face.[30] Accordingly, the permeability of gases across Nafion membranes can be written as

$$p = D_{self}S \tag{5}$$

which is the product of self-diffusivity D_{self} (a kinetic parameter) and sorption solubility S (a thermodynamic factor). The self-diffusivity in the direction α is calculated from the slope of the mean squared displacement of gas molecules as shown in

$$D^{\alpha}_{self} = \frac{1}{2N}\lim_{\Delta t \to \infty}\frac{1}{\Delta t}\left[\sum_{i=1}^{N}(r_i^{\alpha}(t + \Delta t) - r_i^{\alpha}(t))^2\right] \tag{6}$$

The directionally averaged self-diffusion coefficient is given by

$$D_{self} = \frac{D^x + D^y + D^z}{3} \tag{7}$$

3. RESULTS AND DISCUSSION

3.1. Fundamentals of Hydrated Nafion Membranes. To validate our simulations of Nafion systems, the densities of variously hydrated Nafion membranes have been calculated in comparison with experimental data in Figure 2.[31−33] Nafion densities gradually decrease as water content increases due to the swelling effect during membrane hydration. The dynamic property of the aqueous phase is represented by the self-diffusion coefficient, D_{self}, of water in Figure 3. The calculated water diffusion coefficient increases along with the water content and gradually approaches that of the bulk water, i.e., 2.13×10^{-5} cm^2/s at 298.15 K,[34] in good agreement with experimental measurements.[35−37] In particular, a sharp drop of water diffusivity was observed at the dry condition ($\lambda < 6$) from both experiment and simulation, probably attributed to the strong confinement effect of small Nafion micropores on gas mobility. Above the water concentration $\lambda = 6$, a linear correlation can be assigned to water diffusion coefficients. To investigate the relationship between Nafion framework and water transport property, the free volume theory is used for such a polymer system. Free volume V_f is an often used term to relate diffusion D of gas molecules to the porous structure of polymers via[38−42]

$$D = A\exp\left(-\frac{B}{V_f}\right) \tag{8}$$

where A and B are constants for a given gas. In Figure 4, the free volume of simulated Nafion membrane has been calculated and a linear trend is observed with the water content. When the water loadings increase from $\lambda = 4$ to 24, the free volumes of Nafion rise linearly from 0.1 to 0.35 mL/g. This indicates the formation of water channels inside Nafion membrane, as evidenced from Figure 6. Yeager and Steck have proposed that the volume of hydrated Nafion can be divided into three regions: a hydrophobic PTFE backbone region, a hydrophilic aqueous region, and an intermediate region.[43] On the basis of their definition, the free volume of hydrated Nafion in our simulation belongs to the

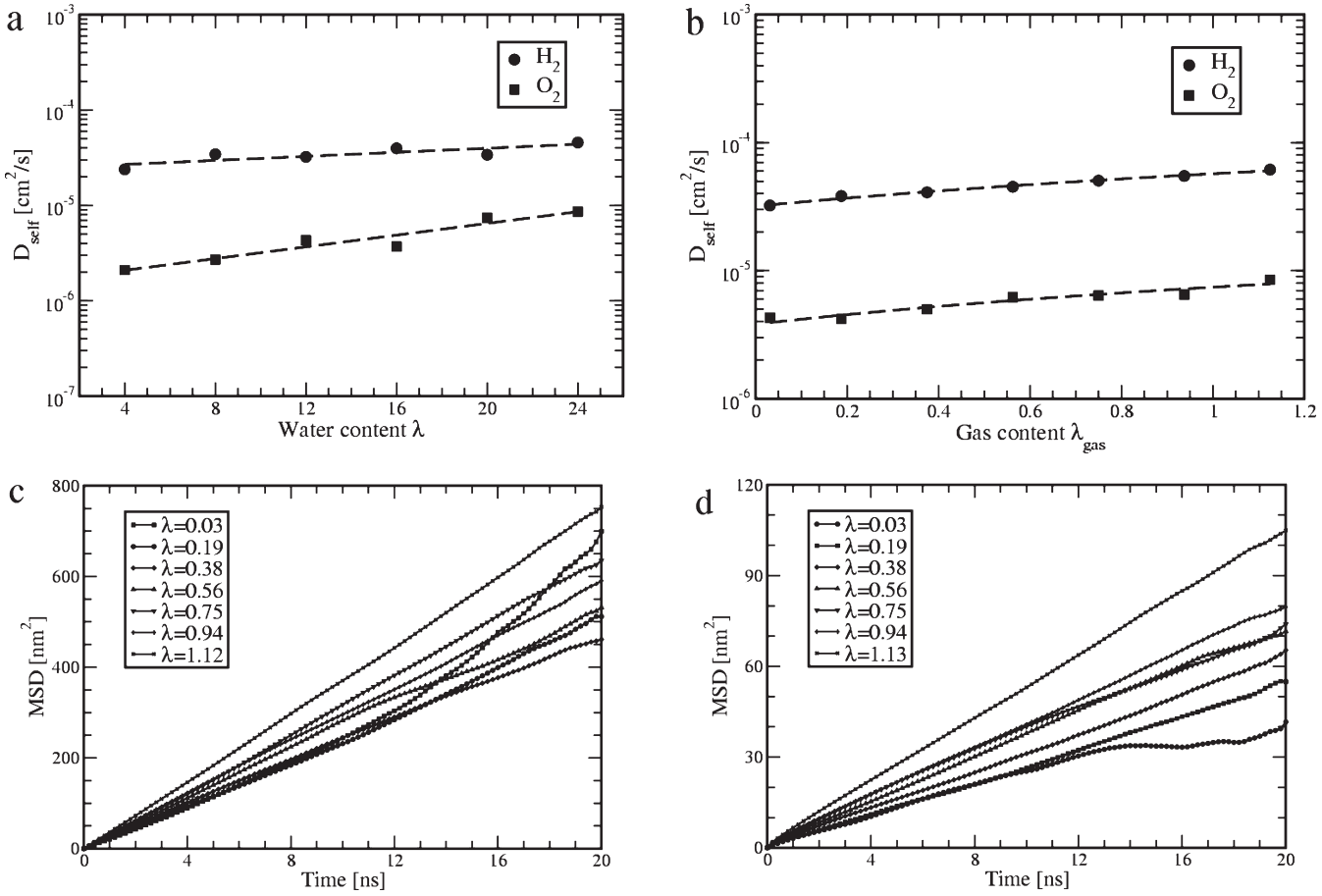

Figure 8. (a) Self-diffusion coefficients of hydrogen and oxygen in hydrated Nafion membranes. The gas content was fixed at a low value of $\lambda_{gas} = 0.03$. Simulations were performed at 353.15 K and 1 bar. The dashed lines are linear fitting of simulation results. (b) Self-diffusion coefficients of hydrogen and oxygen at 353.15 K in hydrated Nafion membrane with a constant water content of $\lambda = 12$. The dashed lines are linear fitting of simulation results. (c) Mean squared displacement of hydrogen at 353.15 K in hydrated Nafion membrane with a constant water content of $\lambda = 12$. (d) Mean squared displacement of oxygen at 353.15 K in hydrated Nafion membrane with a constant water content of $\lambda = 12$.

hydrophilic aqueous region, the volume of which is proportional to the water concentration. It is known from the free volume theory that a linear correlation exists between $\ln D_{self}$ and $1/V_f$. This correlation can be seen from Figure 4. Except D_{self} at dry condition ($\lambda = 4$), diffusion data of water accord well with Nafion free volume, supporting the prediction of the free volume theory.

3.2. Adsorption Properties of Hydrated Nafion Membrane. Figure 5 shows the gas solubility at the zero-pressure limit as a function of water content. For gases H_2, O_2, and N_2, the solubility coefficients decrease with water content, following the sequence of $O_2 > N_2 > H_2$. From gas permeation measurements, Sakai et al. observed a similar trend and found that O_2 solubility coefficient slowly approaches the solubility value in bulk water when the hydration extent of Nafion membrane increases.[5,7,28,44] A close inspection of the simulation snapshot in Figure 6 reveals that gas molecules tend to diffuse through the internal surface of the hydrophobic PTFE backbone of Nafion where microporous structure was recognized. High water content can directly enlarge the sizes of Nafion micropores. The loss of microporous surface results in a decrease of adsorption enthalpy of gas molecules. As a result, gas molecules gradually shift their adsorption locations from the hydrophobic surface of Nafion to the aqueous domain, and the corresponding solubility consequentially approaches the value in bulky water. For Nafion with a constant water content of $\lambda = 12$, the effect of adsorbed gas concentration on the solubility is examined in Figure 5b. Approximately constant solubility again suggests the feasibility of Henry's law in such systems as Nafion.

The linear adsorption isotherms of gases in the hydrated Nafion membrane can be obtained using Henry constant calculated from excess chemical potentials, as shown in eq 4. It is trivial to see that the adsorption amount of gas molecules follows the same order, i.e., $O_2 > N_2 > H_2$, as that of solubility. Using the isotherms of single components, the ideal adsorbed solution theory is employed to predict the adsorption behaviors of gas mixtures.[29] This theory shows that at very low coverage the loading of each component in the mixture is proportional to its partial pressure in the gas phase. At a total pressure of two bars, the adsorption isotherms of H_2/O_2 binary mixtures are shown in Figure 7. As expected, the strong interaction strength of O_2 with Nafion results in a much higher loading than that of H_2 even at the O_2 molar fraction as low as 0.2. The overall O_2 selectivity increases exponentially as a function of the O_2 molar fraction. In the case of H_2/O_2 equal-molar adsorption, the O_2 loading is about 4.4 times as high as that of H_2, independent of the total pressure under ambient conditions. During fuel cell operations, air is often fed into the cell stack instead of pure O_2. In consideration

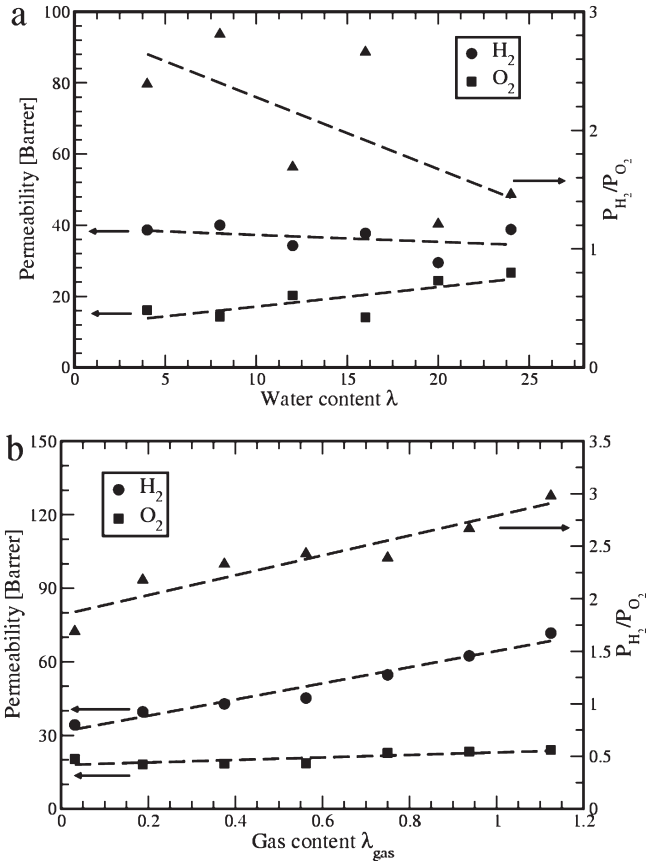

Figure 9. (a) Permeabilities of hydrogen and oxygen through hydrated Nafion membranes at 353.15 K. The gas content was fixed at $\lambda_{gas} = 0.03$; 1 barrer = 10^{-10} mL(STP) cm cm^{-2} s^{-1} cmHg^{-1}. The triangle represents the ratio of H_2 to O_2 permeability. The dashed lines are linear fitting of simulation results. (b) Permeabilities of hydrogen and oxygen through hydrated Nafion membrane with a constant water content of $\lambda = 12$ at 353.15 K. 1 barrer = 10^{-10} mL(STP) cm cm^{-2} s^{-1} cmHg^{-1}. The triangles represent the ratio of H_2 to O_2 permeability. The dashed lines are linear fitting of simulation results.

of the dilution effect of N_2, the adsorption isotherm of $H_2/O_2/N_2$ ternary mixtures with a constant molar ratio of 5:1:4 is computed and depicted in Figure 7b. Due to the low partial pressure of O_2 in the feeding gas, nearly identical loading was found between O_2 and H_2. The adsorption is dominated by N_2, which has a concentration almost three times higher than those of H_2/O_2. This suggests that N_2 is able to efficiently suppress the adsorption of O_2 in hydrated Nafion membranes and protect the fuel cell from fuel crossover.

3.3. Gas Diffusion Properties in Hydrated Nafion Membrane. Figure 8 shows the effects of water content and gas concentration on gas self-diffusivity. The increases of D_{self} observed in both cases indicate that the gas diffusion can be enhanced by these factors. Specifically, H_2 self-diffusivity is 5−10 times higher than O_2 due to its small molecular size and weak interaction with Nafion. Consistent with the experimental findings, D_{self} of O_2/H_2 increases slightly with the water content of the Nafion membranes. The linear correlation of water contents to Nafion free volume suggests the dependence of gas diffusivity on Nafion porous structure. The change of free volume has a more pronounced impact on O_2 than on H_2. The reason for this is that the weak host−guest interaction between H_2 and Nafion cannot restrict H_2 diffusing through the hydrophobic surface. Therefore, the loss of Nafion micropores does not affect H_2 movement in the aqueous region significantly. On the contrary, O_2 has a strong bonding to the hydrophobic surface of Nafion. The growth of free volume effectively releases O_2 from hydrophobic interface of Nafion to the aqueous domains and consequentially leads to a considerable increase of D_{self} at high water content. In this way, D_{self} of O_2 is expected to reach the value in bulk water. Similarly, the high gas concentration may speed up the diffusivity by two means. (1) At high concentration, part of O_2 tends to stay in the aqueous domains as the others occupy most preferable adsorption sites on the hydrophobic surface. (2) Intermolecular collision of gas molecules may enhance gas mobility at moderate adsorbate loadings. For fuel cell operation, these simulations suggest that fuel crossover can potentially increase if high water content is maintained inside the Nafion membrane. Overhydration of Nafion membrane is thus not favored due to concern about the durability of fuel cells.

3.4. Gas Permeabilities in Hydrated Nafion Membrane. According to the solution-diffusion theory, the gas permeabilities have been calculated as a function of water content, as shown in Figure 9a. Because the simulation uncertainty of D_{self} at the low gas content is high, the permeability accordingly shows large fluctuation. Sakai et al. shows that the gas permeability through Nafion membranes greatly depends on the water content and temperature.[7] According to their measurement, at a temperature of 353.15 K and water content of $\lambda = 0-29$, the permeability of O_2 ranges from 10 to 70 barrer and that of H_2 is 40−110 barrer. Our calculated permeabilities of H_2/O_2 agree qualitatively with the permeation measurement.[7] The general trend extracted from Figure 9a is that the H_2 permeability is nearly independent of water content, while O_2 permeability slightly increases. Simulations slightly underestimate this tendency compared to experimental data that show a clear increasing trend for both O_2 and H_2 along with water content.[6,7] The computed ratios of permeabilities between H_2 and O_2 decrease with the water content, ranging around 2. This result agrees well with experimental measurements that concluded the same permeability ratio of H_2 and O_2.[6,7] For the Nafion membrane with a constant water content of $\lambda = 12$, the H_2 permeability increases along the adsorbed concentration while that of O_2 stays nearly constant, as shown in Figure 9b. The permeability ratio of H_2 and O_2 increases from 2 at a low gas loading of $\lambda_{gas} = 0.031\,25$ to 3 at $\lambda_{gas} = 1.125$. The overall higher H_2 permeation than O_2 is attributed to its fast diffusion that compensates for the low solubility in Nafion membranes.

4. CONCLUSIONS

We have employed molecular dynamics methods to simulate gas adsorption, diffusion, and permeation in hydrated Nafion membranes. The models of hydrated Nafion are validated by experiments in terms of material density, Nafion morphology, free volume, and water diffusion.

The adsorption property of hydrated Nafion membranes has been calculated for various gases. Because of the extremely low coverage, the adsorption of gases follows Henry's law. On the basis of this principle, the gas solubilities are computed and a deceasing trend is found with increasing water content. High free volume of hydrated Nafion is the reason for the loss of adsorption sites for gas molecules by eliminating the fraction of small micropores present in the Nafion membrane. Further calculation

of gas adsorption isotherms shows the high O_2 selectivity in H_2/O_2 mixtures, unless N_2 is fed to suppress the O_2 loading. For the dynamic simulations, the diffusion of H_2/O_2 has an increasing trend along with water content and gas concentration. The shift of the gas diffusion path from Nafion hydrophobic surface to the aqueous domain is responsible for the increase of gas diffusivity. As a comparison, the H_2 diffusivity is nearly 1 order of magnitude higher than O_2.

On the basis of the solution-diffusion mechanism, the calculated permeabilities of H_2/O_2 show that O_2 permeability increases with water content, while the H_2 permeability rises with the gas concentration. On average, the H_2 permeability is about two times higher than O_2, agreeing well with experimental observations. For fuel cell operation, our simulations suggest that although water is generally considered as a crucial component to maintain the durability of Nafion membrane, the high water content can, on the other hand, enhance the fuel crossover and cause additional damages to the catalyst layer of fuel cell.

AUTHOR INFORMATION

Corresponding Author

*E-mail: Cheng.huang@nrc-cnrc.gc.ca. Tel.: +1 6042213000, ext. 3050. Fax: +1 6042213001.

ACKNOWLEDGMENT

The authors acknowledge the NRC−Helmholtz Joint Research program for financial support.

REFERENCES

(1) Kordesch, K. V.; Simader, G. R. *Fuel cells and their applications*; Kordesch, K. V., Ed.; VCH Verlagsgesellschaft bmH: Weinheim, Germany, 1996.
(2) Borup, R.; Meyers, J.; Pivovar, B.; Kim, Y. S.; Mukundan, R.; Garland, N.; Myers, D.; Wilson, M.; Garzon, F.; Wood, D.; Zelenay, P.; More, K.; Stroh, K.; Zawodzinski, T.; Boncella, J.; McGrath, J. E.; Inaba, M.; Miyatake, K.; Hori, M.; Ota, K.; Ogumi, Z.; Miyata, S.; Nishikata, A.; Siroma, Z.; Uchimoto, Y.; Yasuda, K.; Kimijima, K. I.; Iwashita, N. *Chem. Rev.* **2007**, *107*, 3904–3951.
(3) Appleby, A. J. *J. Power Sources* **1994**, *49*, 15–34.
(4) Zhang, S.; Yuan, X.; Wang, H.; Mérida, W.; Zhu, H.; Shen, J.; Wu, S.; Zhang, J. *Int. J. Hydrogen Energy* **2009**, *34*, 388–404.
(5) Chiou, J. S.; Paul, D. R. *Ind. Eng. Chem. Res.* **1988**, *27*, 2161–2164.
(6) Broka, K.; Ekdunge, P. *J. Appl. Electrochem.* **1997**, *27*, 117–123.
(7) Sakai, T.; Takenaka, H.; Wakabayashi, N.; Kawami, Y.; Torikai, E. *J. Electrochem. Soc.* **1985**, *132*, 1328–1332.
(8) Chen, P. Y.; Chiu, C. P.; Hong, C. W. *J. Power Sources* **2009**, *194*, 746–752.
(9) Cui, S.; Liu, J.; Selvan, M. E.; Keffer, D. J.; Edwards, B. J.; Steele, W. V. *J. Phys. Chem. B* **2007**, *111*, 2208–2218.
(10) Devanathan, R.; Venkatnathan, A.; Dupuis, M. *J. Phys. Chem. B* **2007**, *111*, 13006–13013.
(11) Jang, S. S.; Molinero, V.; Çagin, T.; Goddard, W. A. *J. Phys. Chem. B* **2004**, *108*, 3149–3157.
(12) Karo, J.; Aabloo, A.; Thomas, J. O.; Brandell, D. *J. Phys. Chem. B* **2010**, *114*, 6056–6064.
(13) Venkatnathan, A.; Devanathan, R.; Dupuis, M. *J. Phys. Chem. B* **2007**, *111*, 7234–7244.
(14) Berendsen, H. J. C.; Grigera, J. R.; Straatsma, T. P. *J. Phys. Chem.* **1987**, *91*, 6269–6271.
(15) Krishna, R.; van Baten, J. M. *Microporous Mesoporous Mater.* **2009**, *125*, 126–134.
(16) Krishnamurthy, M.; Murad, S.; Olson, J. D. *Mol. Simul.* **2006**, *32*, 11–16.
(17) Lindahl, E.; Hess, B.; van der Spoel, D. *J. Mol. Model.* **2001**, *7*, 306–317.
(18) Hess, B.; Kutzner, C.; van der Spoel, D.; Lindahl, E. *J. Chem. Theory Comput.* **2008**, *4*, 435–447.
(19) Berendsen, H. J. C.; van der Spoel, D.; van Drunen, R. *Comput. Phys. Commun.* **1995**, *91*, 43–56.
(20) Van der Spoel, D.; Lindahl, E.; Hess, B.; Groenhof, G.; Mark, A. E.; Berendsen, H. J. C. *J. Comput. Chem.* **2005**, *26*, 1701–1718.
(21) Nose, S. *J. Chem. Phys.* **1984**, *81*, 511–519.
(22) Hoover, W. G. *Phys. Rev. A* **1985**, *31*, 1695.
(23) Blake, N. P.; Petersen, M. K.; Voth, G. A.; Metiu, H. *J. Phys. Chem. B* **2005**, *109*, 24244–24253.
(24) Ban, S.; Vlugt, T. J. H. *Mol. Simul.* **2009**, *35*, 1105–1115.
(25) Widom, B. *J. Chem. Phys.* **1963**, *39*, 2808–2812.
(26) Eslami, H.; Müller-Plathe, F. *Macromolecules* **2007**, *40*, 6413–6421.
(27) Eslami, H.; Muller-Plathe, F. *J. Chem. Phys.* **2009**, *131*, 234904–234908.
(28) Sakai, T.; Takenaka, H.; Torikai, E. *J. Electrochem. Soc.* **1986**, *133*, 88–92.
(29) Myers, A. L.; Prausnitz, J. M. *AIChE J.* **1964**, *11*, 121–127.
(30) Graham, T. *Philos. Mag.* **1866**, *32*, 401–420.
(31) Morris, D. R.; Sun, X. *J. Appl. Polym. Sci.* **2003**, *50*, 1445–1452.
(32) Oberbroeckling, K. J.; Dunwoody, D. C.; Minteer, S. D.; Leddy, J. *Anal. Chem.* **2002**, *74*, 4794–4799.
(33) Takamatsu, T.; Eisenberg, A. *J. Appl. Polym. Sci.* **2003**, *24*, 2221–2235.
(34) Simpson, J. H.; Carr, H. Y. *Phys. Rev.* **1958**, *111*, 1201–1202.
(35) Gong, X.; Bandis, A.; Tao, A.; Meresi, G.; Wang, Y.; Inglefield, P. T.; Jones, A. A.; Wen, W. Y. *Polymer* **2001**, *42*, 6485–6492.
(36) Okada, T.; Xie, G.; Meeg, M. *Electrochim. Acta* **1998**, *43*, 2141–2155.
(37) Zawodzinski, T. A.; Davey, J.; Valerio, J.; Gottesfeld, S. *Electrochim. Acta* **1995**, *40*, 297–302.
(38) Nagel, C.; Günther-Schade, K.; Fritsch, D.; Strunskus, T.; Faupel, F. *Macromolecules* **2002**, *35*, 2071–2077.
(39) Park, J. Y.; Paul, D. R. *J. Membr. Sci.* **1997**, *125*, 23–39.
(40) Haraya, K.; Hwang, S. T. *J. Membr. Sci.* **1992**, *71*, 13–27.
(41) Tanaka, K.; Kita, H.; Okano, M.; Okamoto, K. I. *Polymer* **1992**, *33*, 585–592.
(42) Bendler, J. T.; Fontanella, J. J.; Shlesinger, M. F.; Wintersgill, M. C. *Electrochim. Acta* **2003**, *48*, 2267–2272.
(43) Yeager, H. L.; Steck, A. *J. Electrochem. Soc.* **1981**, *128*, 1880–1884.
(44) Sakai, T.; Takenaka, H.; Torikai, E. *J. Membr. Sci.* **1987**, *31*, 227–234.